Modeling intragranular diffusion in low-connectivity granular media

Robert P. Ewing,[1] Chongxuan Liu,[2] and Qinhong Hu[3]

Received 15 September 2011; revised 20 January 2012; accepted 10 February 2012; published 20 March 2012.

[1] Characterizing the diffusive exchange of solutes between bulk water in an aquifer and water in the intragranular pores of the solid phase is still challenging despite decades of study. Many disparities between observation and theory could be attributed to low connectivity of the intragranular pores. The presence of low connectivity indicates that a useful conceptual framework is percolation theory. The present study was initiated to develop a percolation-based finite difference (FD) model, and to test it rigorously against both random walk (RW) simulations of diffusion starting from nonequilibrium, and data on Borden sand published by Ball and Roberts (1991a,b) and subsequently reanalyzed by Haggerty and Gorelick (1995) using a multirate mass transfer (MRMT) approach. The percolation-theoretical model is simple and readily incorporated into existing FD models. The FD model closely matches the RW results using only a single fitting parameter, across a wide range of pore connectivities. Simulation of the Borden sand experiment without pore connectivity effects reproduced the MRMT analysis, but including low pore connectivity effects improved the fit. Overall, the theory and simulation results show that low intragranular pore connectivity can produce diffusive behavior that appears as if the solute had undergone slow sorption, despite the absence of any sorption process, thereby explaining some hitherto confusing aspects of intragranular diffusion.

Citation: Ewing, R. P., C. Liu, and Q. Hu (2012), Modeling intragranular diffusion in low-connectivity granular media, *Water Resour. Res.*, *48*, W03518, doi:10.1029/2011WR011407.

1. Introduction

[2] Characterizing the diffusive exchange of solutes between bulk water in an aquifer and water in the intragranular pores of the solid phase is still challenging despite decades of study. For organic solutes, the exchange is complicated by such issues as partitioning into various kinds of organic matter [*Huang et al.*, 2003; *Warren et al.*, 2003; *Ten Hulscher et al.*, 2005], bioavailability and biological activity [*Reichenberg and Mayer*, 2006], and nonlinear isotherms [*McGinley et al.*, 1996; *Ran et al.*, 2002]. Exchange of inorganic solutes such as contaminant uranium is complicated by multiple redox states, precipitation in multiple minerals, and interaction with other solutes [*Zachara et al.*, 2007; *Liu et al.*, 2008]. Common to both organic and inorganic solutes is retardation and sequestration via diffusion into intragranular pores in the solid phase [e.g., *Neretnieks*, 1980; *Ball and Roberts*, 1991a; *Werth and Reinhard*, 1997; *Gouze et al.*, 2008].

[3] Diffusion into and out of a porous sphere was described analytically by *Crank* [1975]. A simple system's dynamics might therefore be approximated by considering the granular aquifer to be composed of spheres, accounting for their size distribution, and using a reasonable value for the diffusion coefficient $\mathcal{D}$. Of course, real systems are more complex: the particles are not spherical, intragranular properties may vary with particle size, the particle size distribution may vary in space, large-scale heterogeneities come into play, and so on. Nonetheless, a persistent deviation seen between theory and well-controlled experiments is that, when porous spheres supposedly at equilibrium with a solute are placed in solute-free fluid, early desorption is more rapid than predicted by the analytical solution, and $\mathcal{D}$ appears to slowly decrease over time. As examples see *Pedit and Miller* [1994, Figures 2 and 4], *Harmon and Roberts* [1994, Figures 4–6], *Haggerty and Gorelick* [1995, Figure 4a], *Cornelissen et al.* [1997, Figures 1 and 2], *Fleming and Haggerty* [2001, Figure 6], and *Werth and Hansen* [2002, Figures 1–4]. Linear sorption would present as simple retardation, or a decrease in the diffusion coefficient [*Crank*, 1975], so it cannot explain the change in shape of the curves. The phenomenon has been called "slow sorption" [*Pignatello and Xing*, 1996; *Huang et al.*, 2003; *Warren et al.*, 2003], because an early explanation for it was that solute sorption gradually becomes stronger with long-term contact [*Steinberg et al.*, 1987].

[4] Some portion of the disparity between observation and model may be explained by the particles having a nonuniform size distribution [*Cunningham and Roberts*, 1998]. Other explanations that have been advanced for these disparities include different mineralogies [e.g., *Liedl and Ptak*, 2003], complex sorption/desorption mechanisms [e.g., *Ran et al.*, 2002], and specific kinds or arrangements of intragranular pores [e.g., *Cunningham et al.*, 1997; *Haggerty and*

[1]Department of Agronomy, Iowa State University, Ames, Iowa, USA.
[2]Chemical and Materials Science Division, Fundamental and Computational Science Directorate, Pacific Northwest National Laboratory, Richland, Washington, USA.
[3]Department of Earth and Environmental Sciences, University of Texas at Arlington, Arlington, Texas, USA.

0043-1397/12/2011WR011407

Gorelick, 1998]. While the diffusion may be non-Fickian [e.g., *Dentz and Berkowitz*, 2003; *Gouze et al.*, 2008], reasons for the anomalous behavior are rarely identified. In a previous paper [*Ewing et al.*, 2010] we reviewed some of the explanations, noting that (as pointed out by *Başağaoğlu et al.* [2004]) the disparities could imply that accessible intragranular porosity (that is, intragranular porosity that connects with the exterior) decreases with increasing distance from the exterior. We hypothesized that the underlying cause was low connectivity of the intragranular pores. Using a pore network model of a porous sphere, we confirmed that at low pore connectivity, accessible intragranular porosity decreased with increasing distance from the sphere's surface, while tortuosity increased. Modeling diffusion using random walks (RW) [e.g., *Ewing and Horton*, 2002], we saw that at low intragranular pore connectivity, solute diffused out qualitatively differently from the analysis of *Crank* [1975], deviating similarly to the observations mentioned above.

[5] The RW model was extremely slow, useful for fundamental investigations but not for practical use. We [*Ewing et al.*, 2010] developed equations for accessible porosity ϕ_a and tortuosity τ as functions of both pore connection probability p, and distance l from the sphere's exterior, for use in a finite difference (FD) model. From tortuosity and accessible porosity, the diffusion coefficient as a function of l was calculated by the commonly used [e.g., *Epstein*, 1989] formalism

$$\mathcal{D}_{pm}(l) = \mathcal{D}_{aq}\,\frac{\phi_a(l)}{\tau^2(l)}, \tag{1}$$

where the subscript pm denotes porous medium, and aq denotes free aqueous solution. For $p < 1$, the output of this FD model differed from the *Crank* [1975] analytical solution in the right way: early solute release was faster, and late release slower, than that given by the analytical solution. However, these differences from the analytical model were not great enough to give good agreement with the RW model, and the diffusion coefficient had to be empirically adjusted to sustain agreement with the RW results over the range of connectivities ($1.0 > p > p_c$) examined.

[6] It was unclear why the FD did not better match the RW results. Perhaps the diffusion formulation (equation (1)) is simply incorrect, and a percolation formulation would work better. Within the sphere itself there is no diffusive exchange between the infinite cluster (note: percolation concepts and terminology are presented in section 2) and the finite (edge) clusters, so perhaps it is necessary to calculate diffusion and solute concentrations separately for the two distinct pore spaces (a "split" model) rather than treating them as a single computational unit at each depth within the sphere (a "merged" model). This might be important because near the percolation threshold, most of the accessible pore volume near the sphere's exterior belongs to finite clusters; only a small fraction belongs to the infinite cluster (Figure 1). Accessible pores on the finite clusters (denoted ϕ_f), not being connected to the deeper interior, would presumably desorb fairly quickly. But because there is so little pore volume belonging to the infinite cluster (denoted ϕ_i) near the sphere's surface, solute on the infinite cluster would enter and leave more slowly, constrained by a porosity bottleneck at the edge.

[7] A further motivation for this study was the recognition that considering diffusion starting only from equilibrium constitutes a relatively weak test both of the FD model, and of our underlying conjecture that the slow sorption phenomenon may be diffusion mediated. A more rigorous test would involve (net) in-diffusion followed by (net) out-diffusion at multiple progressive steps toward equilibrium, such that diffusion is examined starting from several different initial conditions.

[8] Finally, it was clear that the FD model would not be useful unless it required few adjustable parameters, and unless it could work with real data (e.g., multiple grain sizes) as well as with theoretical parameters from the RW model.

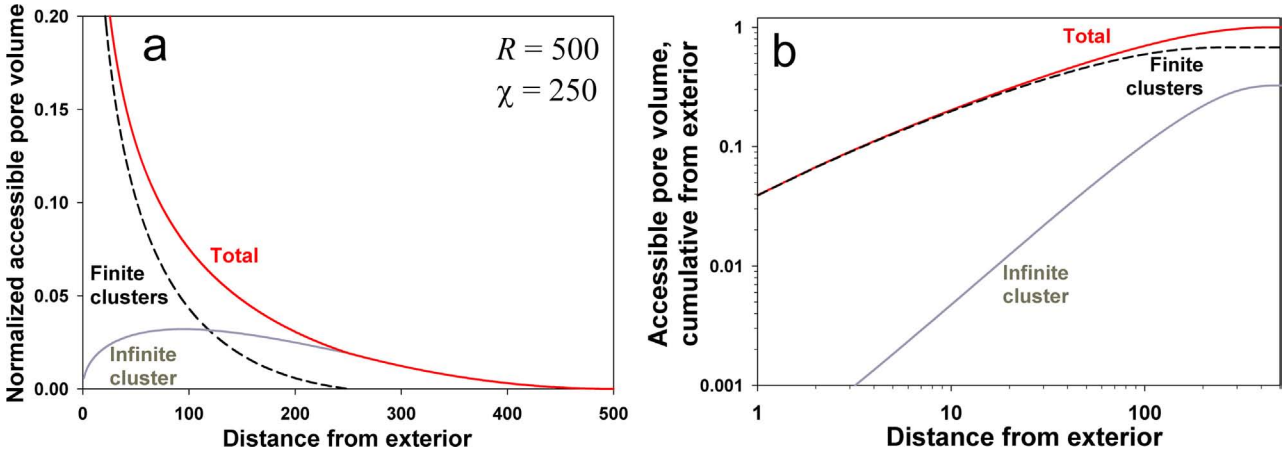

Figure 1. Accessible pore volume as a function of distance l from the sphere's exterior. In this example, $R = 500$ and $\chi = 250$, and approximately 67% of the total accessible pore volume is on finite clusters. (a) Local accessible pore volume (infinite + finite clusters), normalized to the accessible volume of the outermost "shell." (b) Accessible pore volumes, normalized to total accessible pore volume, cumulative from the exterior. Values were calculated using equations (2), (4), and (5).

We therefore reanalyze the classical *Ball and Roberts* [1991b] data on perchloroethene (PCE) sorption in Borden sand, which has also been analyzed with the multirate mass transfer (MRMT) model of *Haggerty and Gorelick* [1995].

[9] Our objectives in this study were therefore to (1) parameterize a FD model using percolation theory concepts, modeling ϕ_i and ϕ_f both separately and together, (2) test the FD model against complex RW simulations, and (3) evaluate the utility of various formulations of the FD model in analyzing data from a classical experiment on PCE uptake into Borden sand.

2. Background and Model Development

2.1. Percolation Theory

[10] A system of pores that have low interconnectivity is best approached as a percolation problem [*Sahimi*, 1994; *Hunt and Ewing*, 2009]. Unfortunately, few hydrologists and soil scientists (the authors included) learned percolation theory as students, so the topic often seems a confusing morass from which we do not know how to extract the relationships we want. Here we present some basic concepts of percolation theory, as background for applying it to diffusive exchange between a porous sphere and the surrounding fluid.

[11] Percolation theory [*Stauffer and Aharony*, 1994] is a mathematical framework for describing the macroscopic properties that emerge in a system composed of many roughly equivalent parts, given the local degree of connection between those parts. In the context of this study, the parts are the individual pores within a single particle (grain, cobble, etc.), and the macroscopic properties of chief interest are the accessible porosity and the intragranular diffusion coefficient. *Ewing et al.* [2010] discussed why it is reasonable to expect that many geological media have low pore connectivity; here we will briefly discuss how some properties emerge as a consequence of low connectivity. Extensive presentations of percolation theory in the context of porous materials are given in the work of *Berkowitz and Balberg* [1993], *Sahimi* [1994], and *Hunt and Ewing* [2009].

[12] Consider a large two-dimensional lattice, for example a brick wall, and suppose that individual sites (e.g., bricks) are colored black with probability p, or white with probability $1 - p$. As p increases from 0, black sites change from being rare and isolated, to occurring in clusters of black sites. Further increases in p increase the mean size of the black clusters, and eventually a threshold is crossed: the black clusters merge to form an "infinite cluster" that spans the entire brick wall, however large it may be. The value of p at which the percolation threshold is reached (the infinite cluster forms) is called p_c, the critical probability. When $p > p_c$, the white sites occur as disconnected clusters, and further increasing p will decrease the mean size of the white clusters until they become rare and isolated. Much of percolation theory can be developed from this simple sketch.

[13] When $p = 1.0$, all sites are black, so all sites are on the infinite cluster. When $p < p_c$, no black site are on the infinite cluster because there is no infinite cluster. The fraction of black sites that belong to the infinite cluster (denoted P, the "power" of the infinite cluster) therefore goes from 0 for $p < p_c$, to 1 at $p = 1$. As it happens, P is described by a simple power law: when $p > p_c$, $P \sim (p - p_c)^{\beta}$. This behavior is independent of (most) details of the lattice: even though square, triangular, cubic, and irregular lattices have different values for p_c, the same power law behavior is seen in all of them, a phenomenon known as universality. The value of β is different in different dimensions, but values are known for both two and three dimensions (Table 1). A consequence of universality is that relationships developed for an easy case, say a square two-dimensional lattice, can then be applied (with some care) to irregular three-dimensional problems.

[14] A useful parameter is the correlation length, χ. For $p < p_c$, χ is essentially the mean radius of the finite clusters, while for $p > p_c$, χ is the mean radius of the holes in the infinite cluster. This has practical implications: if only the black phase is conducting, then pathways through the black infinite cluster are on average separated by a distance χ; this is why χ is also called the "mean separation of paths." χ is known to scale as $\chi \sim |p - p_c|^{-\nu}$, and the presence of the percolation exponent ν (Table 1) generally indicates some form of size scaling. χ functions as a characteristic length, and we find that systems behave homogeneously at length scales $L \gg \chi$, while behavior at scales less than χ is typically scale dependent. Because $\chi \to \infty$ as $p \to p_c$, the only operational length scale at p_c is the system size.

[15] Suppose a system is near p_c, and we want to know the length of a path between two given sites on the same cluster. The straight line or Euclidean distance, l, can be calculated trivially, but the connecting pathway, proceeding from site to connected site, is more complex. The length of this path is called the chemical distance, λ, because in a porous medium, with sites corresponding to pores, this is the shortest path available to a molecule traveling between the two sites. The path is fractal at scales greater than the scale of individual sites but less than χ; for these distances λ is related to the Euclidean distance as $\lambda \sim l^{D\min}$ (Table 1). The ratio λ/l is therefore the tortuosity τ, the value of which must be scale dependent at scales greater than a single pore and less than χ [*Ewing et al.*, 2010].

[16] As a final illustration, consider conduction through the infinite cluster. If $p = 1$, the system's conductivity, g, is clearly determined by the distribution of conductivities. But as p decreases toward p_c, the individual conducting pathways become more tortuous (with D_{min}), while the separation between individual pathways becomes greater (with ν). At some point [*Hunt*, 2004; *Ewing and Hunt*, 2006] the topological considerations become more important than the conductivity distribution, and the system's

Table 1. Fundamental Percolation Exponents Discussed in This Study

Exponent	Value in 2-D	Value in 3-D	Meaning
β	5/36[a]	0.41	Defines the fraction of the medium that is on the infinite cluster (the "power" of the infinite cluster).
ν	4/3	0.88	Defines χ, the fundamental length scale near p_c. Indicates size-scaling.
D_{min}	1.13	1.34	Fractal dimension of the chemical path between two points on the same cluster; related to tortuosity.
μ	1.31	2.0	Describes conductivity near p_c in an infinite medium.

[a]Values that are known analytically are given as fractions; decimal values are numerical estimates.

conductivity is found to scale with proximity to the percolation threshold as $g \sim (p - p_c)^{\mu}$ (Table 1).

[17] Instead of having sites be black with probability p ("site percolation"), we could have had bonds (the connections between adjacent sites) being active with probability p ("bond percolation"). The values of the critical probabilities, and of the prefactors needed to convert the scaling relationships to equalities, are specific to the lattice used (square, honeycomb, etc.), and whether it is site or bond percolation that obtains. However, the scaling relationships we have shown hold generally across these as well as other considerations. Our RW model uses bond percolation on a simple cubic lattice, so we know that $p_c \approx 0.2488$ [*Stauffer and Aharony*, 1994]. In a physical system (e.g., Borden sand), we do not know either p or p_c, so different methods must be found to work with percolation concepts. Both conceptual and physical systems are considered in this study.

2.2. Model Development

[18] When accessible porosity is not uniform, a FD model needs local values of accessible porosity in order to convert between concentration (the driving force) and solute mass. Our FD model therefore requires equations giving local values of both accessible porosity, ϕ_a, and the diffusion coefficient, $\mathcal{D}_{pm}$. When the sphere has low pore connectivity, these parameters vary as functions of both the proximity to the percolation threshold (i.e., with $p - p_c$), and the intragranular distance l to the sphere's exterior. We address the accessible porosity first. Recall that the percolation exponent β gives the fraction of active sites that are on the infinite cluster, and in an infinite system, only sites on the infinite cluster would be accessible over great distances. Meanwhile, scaling with distance occurs for distances $l < \chi$. The value of χ for a system above the percolation threshold is given by $\chi = a\,(p - p_c)^{-\nu}$, with a being a system-specific prefactor. The β and ν exponents combine to give an exponent $-\beta/\nu$, which governs how accessible porosity varies with distance from the exterior. If p and p_c are known (e.g., when comparing the FD model with the RW model) then a is a fitting parameter; for a physical system (e.g., the Borden sand) we instead consider χ to be a fitting parameter.

[19] At distances $l > \chi$, ϕ_a takes a constant plateau value which we designate ϕ_p. Closer to the exterior, ϕ_a decreases with an exponent $-\beta/\nu$. Equating these at $l = \chi$ defines a prefactor $b \equiv \phi_p\,\chi^{\beta/\nu}$, so

$$\phi_a(l) = \begin{cases} b\,l^{-\beta/\nu} & l < \chi \\ \phi_p & l \geq \chi \end{cases}, \tag{2}$$

where the scaling with distance shows up through both the exponent ν, and the crossover in scaling at $l = \chi$ (Figure 1). With these relationships, and given χ and ϕ_p for a sphere of radius R, then ϕ_a for the whole sphere can be calculated as

$$\phi_a = \frac{\phi_p}{R^3}\left[(R-\chi)^3 + 3\chi^{\beta/\nu}\int_{R-\chi}^{R}[R-r]^{-\beta/\nu} r^2 dr\right], \tag{3}$$

and given any three of [R, χ, ϕ_p, ϕ_a], we can calculate the fourth.

[20] When modeling the sphere without distinguishing between the infinite and finite clusters (the "merged" model), equation (2) suffices to describe the porosity distribution. But when modeling the infinite and finite clusters as separate systems operating in parallel (the "split" model), their accessible porosities must be treated separately. All accessible porosity must be on either the infinite cluster (ϕ_i) or those finite clusters intersecting the edge (ϕ_f): $\phi_a = \phi_i + \phi_f$. Accessible porosity on the infinite cluster varies with intragranular distance l to the grain's exterior as

$$\phi_i(l) = \begin{cases} \phi_p (l/\chi)^{\beta/\nu} & l < \chi \\ \phi_p & l \geq \chi \end{cases}. \tag{4}$$

[21] By definition, all accessible pores at distances $l > \chi$ belong to the infinite cluster (Figure 1). Consequently, accessible porosity due to the finite clusters, ϕ_f, is nonzero only for $l < \chi$, and is given by the difference between equations (2) and (4):

$$\phi_f(l < \chi) = \phi_p\left[\left(\frac{\chi}{l}\right)^{\beta/\nu} - \left(\frac{l}{\chi}\right)^{\beta/\nu}\right]. \tag{5}$$

When the sphere is small relative to the correlation length (i.e., when $R < \chi$), there is no infinite cluster. In this case we consider that the split and merged models are identical.

[22] The FD model also requires a percolation-based estimate of the diffusion coefficient, $\mathcal{D}_{pm}$. As with ϕ_a, two distinct scaling issues apply: scaling with distance l from the sphere's exterior, and scaling with $p - p_c$, the proximity to the percolation threshold. As with porosity, diffusion scaling with distance has a crossover at $l = \chi$, and is known to take the form [*Stauffer and Aharony*, 1994]

$$\mathcal{D}_{pm}(l) \sim \min(l,\chi)^{-\vartheta}, \tag{6}$$

where the exponent $\vartheta \equiv (\mu - \beta)/\nu \approx 1.807$ in 3-D. As we would expect, this distance-scaling exponent has the exponent ν in the denominator.

[23] The second kind of scaling, scaling with $p - p_c$ for distances $l > \chi$, was seen by *Ewing et al.* [2010] to follow

$$\mathcal{D}_{pm}(p) \sim (p - p_c)^{\psi}. \tag{7}$$

They gave the exponent $\psi \approx 1.42$ in 3-D, and conjectured that $\psi \equiv (2 + \vartheta)/2\ D_{min}$. On the other hand, *Havlin and Ben-Avraham* [2002] and *Stauffer and Aharony* [1994] give the exponent $\psi \equiv 2\nu - \beta$ ($\approx$1.35 in 3-D) for $p < p_c$, which is to say, for finite clusters near criticality. This exponent can be interpreted as meaning that diffusion is restricted to a single pathway (on average) through each area χ^2 (because the mean distance between paths scales with the exponent $-\nu$), and is directly proportional to the fraction of the porosity that is on the infinite cluster (controlled by the β exponent). For comparisons against the RW model, we ran the FD model with both values of ψ.

[24] Because diffusion and conductivity are related, one might expect that the relevant exponent would be μ rather than ψ. The short explanation is that in our porous spheres

we have diffusion on both the infinite cluster and the finite clusters; when diffusion is restricted to the infinite cluster, the μ exponent is appropriate. A fuller explanation [e.g., *Stauffer and Aharony*, 1994] is beyond the scope of this paper.

[25] Equation (7) is problematic in terms of actual implementation, most obviously because the endpoints are wrong. For example, we may want $\mathcal{D}_{pm}$ at $p = 1.0$ to take some known value (denoted $\mathcal{D}_k$), and can easily normalize to obtain it. But equation (7) would also give $\mathcal{D}_{pm} = 0$ at $p = p_c$, which is only asymptotically true for infinite systems, in contrast to the finite spheres we are considering. Specifically, if we are working with a grain of size $R \leq \chi$, all intragranular pores lie within the region of decreasing porosity and increasing tortuosity (Figure 1). Within this region, all values of p between p_c at the low end, and $p_c + (R/a)^{-1/\nu}$ at the high end, should give identical values of the diffusion coefficient (combining both the infinite and finite clusters): all of these systems behave essentially identically within a distance $l < \chi$ of the exterior [*Ewing et al.*, 2010, Figure 10]. We therefore modify equation (7) to

$$\mathcal{D}_{pm}(p) \sim (p^* - p_c)^{\psi}, \tag{8a}$$

where

$$p^* \equiv \max\left[p,\ p_c + \left(\frac{R}{a}\right)^{-1/\nu}\right]. \tag{8b}$$

This modification is further justified in section 5. Combining the two kinds of scaling (equations (6) and (8)) and normalizing to the known $\mathcal{D}_k$ at $p = 1.0$ gives

$$\mathcal{D}_{pm}(p,l) = \mathcal{D}_k\left[\frac{p^* - p_c}{1 - p_c}\right]^{\psi}\begin{cases} l^{-\vartheta} & l < \chi \\ \chi^{-\vartheta} & l \geq \chi \end{cases}. \tag{9}$$

[26] The above discussion involves an artificial system for which $p - p_c$ is known. In contrast, a physical system's proximity to the percolation threshold is not generally known. In this case we combine the several unknowns, defining

$$\mathcal{D}_0 \equiv \mathcal{D}_k\left[\frac{p^* - p_c}{1 - p_c}\right]^{\psi}, \tag{10}$$

which allows us to treat $\mathcal{D}_0$ as our second fitting parameter (after χ). The local diffusion coefficient is then simply given as

$$\mathcal{D}_{pm}(l) = \mathcal{D}_0\begin{cases} l^{-\vartheta} & l < \chi \\ \chi^{-\vartheta} & l \geq \chi \end{cases}. \tag{11}$$

3. Methods

3.1. Random Walk Simulations

[27] *Ewing et al.* [2010] used a random walk (RW) model to simulate diffusion of a solute from a porous sphere of radius R lattice units. The random walkers were initially emplaced randomly and then allowed to diffuse out, modeling the case in which a saturated porous sphere is initially at diffusive equilibrium with the surrounding fluid (i.e., solute concentrations are the same everywhere, both inside and outside the sphere), then is moved to a solute-free fluid. The RW model agreed with *Crank*'s [1975] solution at high connectivity ($p = 1.0$), and with percolation theory at low connectivity ($p = p_c$), giving it credence as a standard against which to test the FD model.

[28] In this work we extended the RW model to simulate the case of a water-saturated but initially solute-free porous sphere (initial internal concentration $C = 0$) being immersed in an infinite reservoir of a solution of concentration $C_0 > 0$, then returned to a solution with $C = 0$ before equilibrium is reached (i.e., while mean intragranular $C/C_0 < 1.0$). As realized in the RW model, the intragranular porespace is initially free of random walkers: all walkers start outside the sphere. At mean intragranular relative concentrations $C/C_0 = 10\%$, 20%, 50%, and 90%, the model takes a "snapshot," recording the number of elapsed time steps and the location of all walkers, then diffusion continues until $C/C_0 > 90\%$. (Note that in contrast to normal usage for breakthrough curves, here C/C_0 refers to the mean relative solute concentration ratio inside the porous sphere.) Afterward, for each of these concentrations, the system is restored to the snapshot configuration, but walkers currently outside the sphere are removed, as are all remaining walkers upon exiting the sphere. Diffusion proceeds until all random walkers have exited the sphere. This way, one in-diffusion episode is used to initialize out-diffusion episodes from four different nonequilibrium "flip points." Despite this efficiency, each realization took much more time than a simple out-diffusion simulation with identical parameters. Simulations with $R < 500$ were run on a personal computer, but the more CPU-intensive $R = 500$ simulations were run on the parallel supercomputer s*pokane* at the Environmental Molecular Sciences Laboratory (EMSL), Pacific Northwest National Laboratory (PNNL). 100 realizations were run for each combination of R and p.

3.2. Finite Difference Model For Comparison With RW Model

[29] Diffusion in spherical coordinates is usually described by

$$\frac{\partial C}{\partial t} = \mathcal{D}\left(\frac{\partial^2 C}{\partial r^2} + \frac{2}{r}\frac{\partial C}{\partial r}\right), \tag{12}$$

where $r \equiv R - l$ is the distance from the sphere's center. Making the substitution $c \equiv rC/C_0$ [*Crank*, 1975] normalizes the concentration to our reference concentration, and changes equation (12) to

$$\frac{\partial c}{\partial t} = \mathcal{D}\frac{\partial^2 c}{\partial r^2}, \tag{13}$$

the same form as the simpler one-dimensional diffusion equation. We discretize the sphere into shells of thickness Δr, and time into periods of duration Δt. Putting equation (13) into finite difference (FD) form and making the

substitution $d \equiv \mathcal{D}\Delta t/(\Delta r)^2$, we rearrange it to obtain [*Crank*, 1975; *Press et al.*, 1992]

$$-dc_{j-1,t+1} + (2+2d)c_{j,t+1} - dc_{j+1,t+1} = dc_{j-1,t} + (2-2d)c_{j,t} + dc_{j-1,t}, \quad (14)$$

where the subscript j denotes radial position, and t time. Note that all terms on the left-hand side are at time $t + 1$; while the right-hand side is all at time t. These equations form a tridiagonal matrix, which is readily solved with the Thomas algorithm [e.g., *Press et al.*, 1992].

[30] Where the diffusion coefficient $\mathcal{D}$ changes with position (equation (9)), a mean value is calculated by integrating $\mathcal{D}_{pm}(l)$ over the thickness of the shell, and dividing by Δr to get an effective mean value. Porosity enters into equation (14) indirectly, because solute concentration inside the sphere is solute mass per unit pore volume. The intragranular porosity changes with distance from the exterior, so the model tracks solute mass and intragranular pore volume as distinct variables at each location, calculating concentration from them as needed. The simulation starts with a large concentration gradient at time $t = 0$, but gradients decrease to near zero as equilibrium is approached, so we used a small initial time step $\Delta t = 1.0$, and obtained subsequent time steps by multiplying the previous time step by 1.01.

[31] The initial condition was $C = 0$ at $t = 0$ and $l > 0$. The exterior boundary condition was $C = C_0$ at $t > 0$, changing to $C = 0$ after the flip time. Solute uptake and release were expressed in terms of the mean intragranular concentration, C/C_0. The merged model calculated porosity via equation (2), while the split model used equations (4) and (5). Model inputs were the sphere radius R, the shell thickness Δr, the connection probability p, the critical probability p_c, the known diffusion coefficient for $p = 1.0$ ($\mathcal{D}_k = 1/6$ (lattice units)^2 (time steps)$^{-1}$; *Ewing and Horton* [2002]), and the prefactor a, the model's sole fitting parameter. The value of ϕ_p was estimated from χ and the value of ϕ_a at $l = 1$ and $p = p_c$ (0.744 in the RW model).

3.3. Borden Sand Data

[32] The experiment analyzed here is described in the work of *Ball and Roberts* [1991a, 1991b], with additional details given in *Ball*'s [1989] dissertation. Briefly, uncontaminated Borden sand was sieved into 7 size classes; a bulk nonsieved sample was also retained. Replicates of these eight samples were placed in batch reactors and exposed to aqueous PCE, uptake of which was measured over some 100 days. For each size class they measured the particle size range, intragranular porosity, solid/liquid ratio (S/L), and long-time "ultimate fractional uptake" K_d^{ult}. They also measured uptake at intermediate times, from which they calculated apparent uptake K_d^{app}. Solute uptake was presented in terms of K_d^{app}/K_d^{ult}, which (assuming no instantaneous uptake) can be calculated from the initial (C_0), equilibrium (C_e), and intermediate time ($C(t)$) reservoir concentrations as (see their equations (9a) and (9b)):

$$\frac{K_d^{app}}{K_d^{ult}} = \frac{[C_0/C(t)] - 1}{(C_0/C_e) - 1}. \quad (15)$$

A useful parameter in analyzing these data is *Crank*'s [1975] α parameter, the ratio of the reservoir (batch reactor) fluid volume to the (accessible) intragranular pore volume as adjusted for sorption: $\alpha = 1/[K_d^{ult} \times (S/L)]$. The reservoir concentration asymptotically approaches an equilibrium value $C_e = C_0\ \alpha/(1 + \alpha)$. The Borden sand's sorption isotherm was linear within the experimental range of PCE concentrations [*Ball and Roberts*, 1991a].

[33] We digitized uptake (K_d^{app}/K_d^{ult}) data from appendix E of *Ball* [1989]. For each size class we used the geometric mean of the maximum and minimum radii as the characteristic radius. Experimental values of the S/L ratio ranged from 0.22 to 2.0 g mL^{-1} [*Ball and Roberts*, 1991a]; to calculate α for each size class we used the midpoint of the range given for that class. Uptake data for the bulk sand were provided by W. P. Ball (personal communication, 2011). The mean of the absolute values of the differences between our digitized bulk sand data and those provided by Ball, relative to Ball's values, was less than 1% for both time and K_d^{app}/K_d^{ult}. Parameter optimization was done for each size class at the mean α that *Ball and Roberts* [1991b] reported for that size class. Bulk sand predictions were generated by making an uptake curve for each size class at the α reported for bulk sand (approximately 0.932), and combining these curves as described by *Haggerty and Gorelick* [1995].

3.4. Finite Difference Model for Analysis of Borden Sand Data

[34] For analysis of the Borden sand data, the finite difference (FD) model was modified in a few significant ways. We used only the merged model, and calculated the local diffusion coefficient using equation (11). Time was in seconds rather than unitless "time steps," and distance in mm rather than "lattice units." Because *Ball and Roberts*' [1991a, 1991b] reactors had finite fluid volume, the reservoir concentration was iteratively adjusted within each time step to maintain mass balance. Where porosity was not uniformly distributed, the FD model treated sorption as being locally proportional to accessible pore volume, in contrast to analytical solutions which assume spatially uniform properties.

[35] Analysis of the Borden sand data used several models differing in number and handling of the fitting parameters (Table 2). The *Ball and Roberts* [1991b] single-sphere approximation, denoted $1\mathcal{D}$BR, treats the bulk sand as having a single characteristic particle radius given by the Sauter mean particle radius, and fits a single diffusion coefficient to the bulk sand data using *Crank*'s [1975] finite-reservoir series solution. The other six models used the published particle size and intragranular porosity data in a separate FD solution for each of the size classes. These FD models ranged from forcing $\chi = 0$ and fitting a value of $\mathcal{D}_0$ simultaneously to all seven size classes (model $1\mathcal{D}$), to fitting a unique $\mathcal{D}_0$ and χ for each of the seven size classes (model $7\mathcal{D}7\chi$). Model $7\mathcal{D}$ is equivalent to *Haggerty and Gorelick*'s [1995] MRMT model, and this model gave identical results when implemented using *Crank*'s [1975] solution and the FD model.

4. Results

[36] Our previous work [*Ewing et al.*, 2010] favored the interpretation $\psi \equiv (2 + \vartheta)/(2\ D_{min}) \approx 1.42$ in 3-D, but the

Table 2. Summary of Models Used to Simulate the Borden Sand Experiment

Model	Number of Sphere Sizes	Number of Fitting Parameters			Error Sum of Squares for 7 Size Classes	Error Sum of Squares for Bulk Sand
		$\mathcal{D}_0$	χ	Total		
$1\mathcal{D}$BR[a]	1	1	0	1	–	0.1551
$1\mathcal{D}$	7	1	0	1	4.0484	0.1377
$7\mathcal{D}$[b]	7	7	0	7	1.8650	0.1376
$1\mathcal{D}1\chi$	7	1	1	2	3.8345	0.1494
$7\mathcal{D}1\chi$	7	7	1	8	1.3191	0.1344
$1\mathcal{D}7\chi$	7	1	7	8	2.8345	0.1331
$7\mathcal{D}7\chi$	7	7	7	14	1.2975	0.1327

[a]Equivalent to the *Ball and Roberts* [1991b] single-sphere fit.
[b]Equivalent to the *Haggerty and Gorelick* [1995] seven sphere composite MRMT prediction.

more rigorous tests of the present study support $\psi \equiv 2\nu - \beta \approx 1.35$ in 3-D. This more standard value [*Havlin and Ben Avraham*, 2002; *Stauffer and Aharony*, 1994] gives a better match to the RW results for diffusion starting from nonequilibrium, especially as $p \rightarrow p_c$ (comparison not shown). For brevity, only the $\psi \equiv 2\nu–\beta$ results are reported and discussed.

4.1. Comparison With RW Model

[37] The best overall match between the FD and RW output was seen when $a = 0.095$, slightly greater than *Ewing et al.*'s [2010] $a = 0.07$ for porosity, but less than the $a = 0.21$ that they used for tortuosity. Note that a is adjustable only within fairly constrained bounds, because it has a clear physical meaning, and its value can be estimated independently of simulations such as these. All subsequent comparisons of the RW and FD models use $\psi \approx 1.35$ and $a = 0.095$.

[38] With no other adjustable parameters, the FD model results closely matched the RW results across all values of p, and for both net in-diffusion and net out-diffusion. We first examine results for the case of $p = 1.0$, for which $\chi \approx 0$ and so the merged and split models are identical. This is shown (Figure 2) in all combinations of linear and logarithmic axes, to acquaint the reader with the various forms in which these data can be displayed. With both axes linear (Figure 2a), the plot of C/C_0 over time resembles a breakthrough curve (BTC) with a pulse input of several pore volumes [e.g., *Brusseau et al.*, 1997]. Recall that the concentrations being plotted are the mean concentration inside the sphere, rather than effluent concentrations. At low pore connectivity, extremely long times can be required to attain internal mean concentrations $C/C_0 \geq 90\%$, so it can be useful to use logarithmic time axes (Figure 2b). When plotted with linear time and logarithmic relative concentration (Figure 2c), out-diffusion limbs starting from all four flip points appear parallel; we shall make use of this later. Finally, when both axes are logarithmic (Figure 2d), the entire range is visible, and larger-scale patterns emerge. While each alternative presentation in Figure 2 has advantages, in the interest of brevity we present further results only in the log-log format.

[39] The agreement between RW and FD models remains quite good for $p < 1.0$ (Figure 3), with all curves matching well in shape. There is little visible difference between the merged and split models, except for slight separation in the net out-diffusion legs in Figures 3b and 3c. With no substantive difference between the two models, the merged model is to be preferred for the sake of simplicity. Again, we emphasize that the only change in input between FD runs was the value of p; there are no empirically adjusted parameters beyond a, which was held constant in Figures 2 and 3.

[40] The main difference between the RW and FD models (Figure 3) involves the timing of the flip points, so we compared the FD flip times to the RW flip time distributions (Figure 4). FD flip times range between the 75th and 95th percentiles for $p = 1.0$ (Figure 4a), showing that the FD model is in reasonable agreement with the RW model (as also seen in Figure 2). For $p = 0.255$ (Figure 4b) the first FD flip point is quite late, but the last two are early. At $p = 0.25$ (Figure 4c), the merged model performs slightly better than the split model on the timing of the first two flip points. Finally, when $p = p_c$ (Figure 4d), the agreement is quite good. The overall pattern is that the FD model performs quite well at $p = 1.0$ and $p = p_c$, but is less accurate slightly above the threshold. We suspect that the underlying cause of this timing mismatch is that the discrete nature of the models introduces some artifacts. *Ewing et al.* [2010] mentioned artifacts due to the cubic connectivity of the RW model; analogous issues arise in the FD model. The greatest difference in flip points is found at values of p for which χ takes quite small values: at $p = 0.27$, $\chi = 2.8$, and at $p = 0.255$, $\chi = 8.3$. Our implementation of the FD scheme used uniform layer thicknesses, and rounding these small values of χ could introduce significant changes.

[41] As noted above, the out-diffusion limbs in Figure 2c appear to have the same slope, showing that the diffusion coefficient appears to follow approximately the same trajectory in each case. This slope can be used to calculate an apparent diffusion coefficient $\mathcal{D}_{app}$ that applies to the sphere as a whole:

$$\mathcal{D}_{app} = -\frac{R^2}{\pi^2}\frac{\Delta \ln (C/C_0)}{\Delta t}. \tag{16}$$

As discussed in the work of *Ewing et al.* [2010], $\mathcal{D}_{app}$ is expected to decrease with time, asymptotically approaching the "correct" value. The calculated $\mathcal{D}_{app}$ shows nearly identical behavior for both the RW and FD models when shown as a function of time from the flip points (Figure 5), further confirming that the FD model captures the essentials of the RW model. For $p = 1.0$ (Figure 5a), when starting from an earlier flip time (say, $C/C_0 = 10\%$ versus 90%), $\mathcal{D}_{app}$ decreases more quickly after the first few hundred time steps, but the same final value, approximately 1/6, is reached

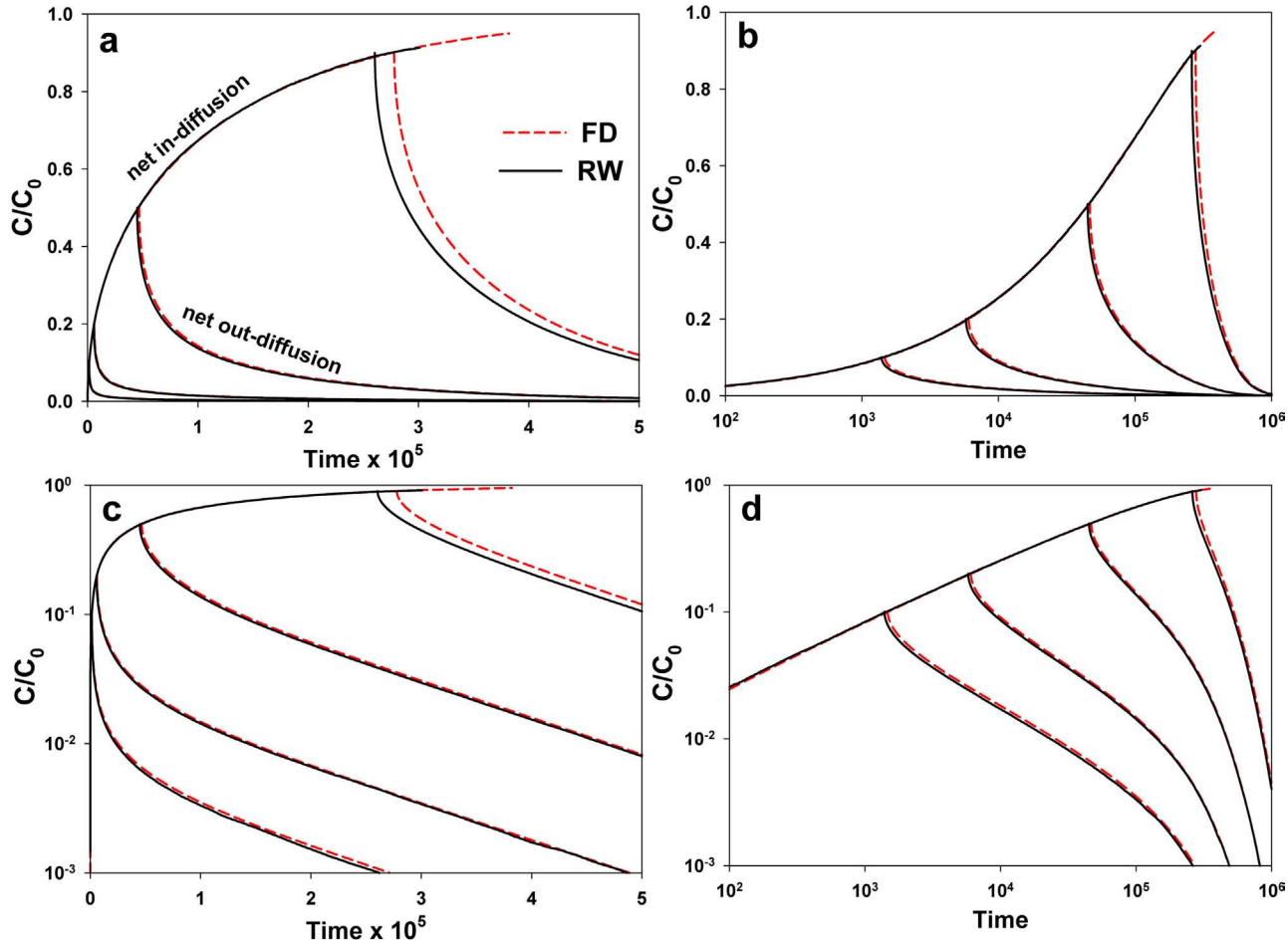

Figure 2. Comparison of finite difference (FD) and random walk (RW) simulations of relative internal concentration (C/C_0, the mean relative solute concentration ratio *inside* the porous sphere) as a function of time, for a sphere of $R = 500$ and $p = 1.0$. All plots show the same data, with (a) both axes linear, (b) a logarithmic time axis, (c) a logarithmic concentration axis, and (d) both axes logarithmic.

regardless of flip point. But for $p = p_c$ (Figure 5b), later flip points yield lower final estimates of $\mathcal{D}_{app}$. In other words, as the solute distribution inside the sphere approaches equilibrium, the sphere's apparent diffusion coefficient decreases, because late-time diffusion is controlled by the lower diffusion coefficient deeper inside the sphere. This decrease in the final value of $\mathcal{D}_{app}$ with increasing time is characteristic of the "slow sorption" phenomenon.

[42] The issue of the extent to which a nonequilibrium starting condition affects the progress of the out-diffusion is further examined in Figure 6, in which the concentrations at the flip times have all been normalized to 1.0; the in-diffusion is also shown. For the high-connectivity case (Figure 6a), the 10% flip point line differs from the later flip point lines mainly in the middle section; all the lines begin and end together. In contrast, the low-connectivity case (Figure 6b) shows a much stronger separation, with the lines rejoining (if at all) much later, at $C/C_0 < 10^{-6}$. Now consider Figure 6b in the context of slow sorption: let the various out-diffusion lines all represent the same quantity of solute that, having aged in place, is increasingly close to internal equilibrium. Because the curves are similar, appearing to have been simply shifted to the right on the time axis with increasing time, they could reasonably be interpreted as differing only in the diffusion coefficient. That is, in a medium having intragranular pore connectivity near the percolation threshold, the closer the system is to equilibrium when out-diffusion starts, the lower its apparent diffusion coefficient. Alternatively, because sorption with a linear isotherm presents as a simple decrease in the diffusion coefficient, the lines could also be interpreted as showing a sorption coefficient that increases with time. In other words, Figures 5b and 6b show that low intragranular pore connectivity is a possible explanation for the aging or "slow sorption" phenomenon.

4.2. Comparison With Borden Sand Data

[43] The *Ball* [1989] bulk sand data are noisy for measurements after the first month (Figure 7), so every model's bulk sand prediction error term is dominated by late-time data scatter. As Figure 7a (similar to *Haggerty and Gorelick*'s [1995, Figure 4a]) shows, the $1\mathcal{D}$BR fit differs from the $7\mathcal{D}$ prediction primarily at times earlier than 30 days: the models agree well at later times. But despite model

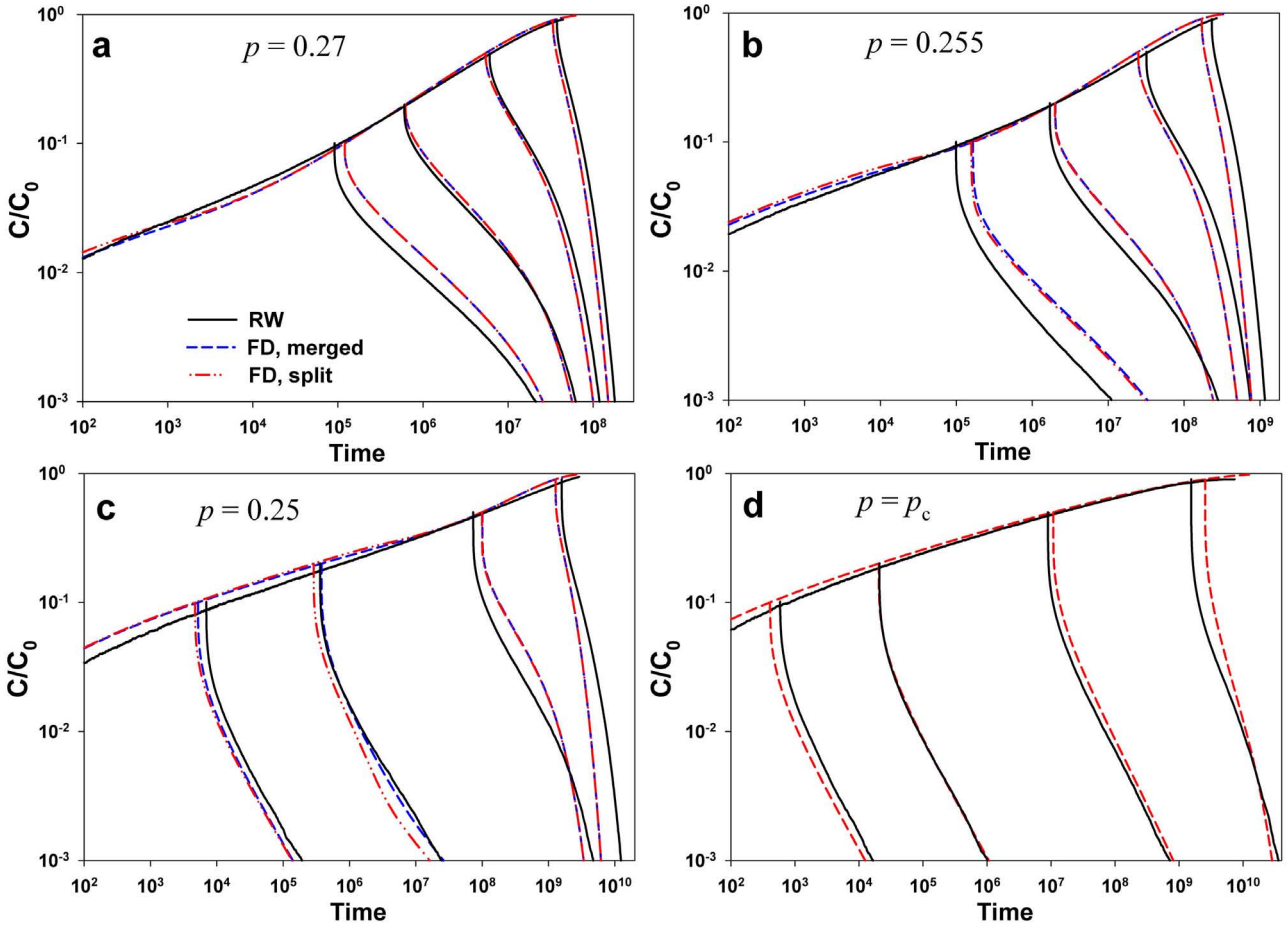

Figure 3. Comparison of random walk (RW) simulations, and both merged and split finite difference (FD) models, of relative internal concentration C/C_0 as a function of time for a sphere of $R = 500$ and $p =$ (a) 0.27, (b) 0.255, (c) 0.25, and (d) p_c.

$7\mathcal{D}$'s improved accord with the data at early times, its error term is only 11% less than the $1\mathcal{D}$BR single-sphere fit (Table 2). So because of late-time scatter, even an appreciable improvement in prediction may yield only a small reduction in the error term. For this reason we also present an error term for the fitting runs (Table 2), representing the sum of squared residuals for the 154 observations across all 7 size classes. According to the AIC_c [*Hurvich and Tsai*, 1995], the best model using the bulk sand error term is $1\mathcal{D}$; using the size class error term, the best model is $7\mathcal{D}1\chi$.

[44] All models that permitted $\chi > 0$ converged to a nonzero value for χ. The fitted values of χ from model $7\mathcal{D}7\chi$ were quite small, between 3 and 10 μm (from about 1% to 11% of a particle's radius), but finite cluster pore volume contributed 9.6% (largest size class) to 41.7% (smallest size class) of the accessible pore volume. The effect of nonzero values of χ on early PCE uptake was striking (Figure 7). The best matches, both visually and according to their error terms, were given by models $7\mathcal{D}1\chi$ and $7\mathcal{D}7\chi$ (Table 2), which were indistinguishable from each other (Figure 7b) and had error terms lower than the $1\mathcal{D}$BR model by 13.3% and 14.5%, respectively.

[45] With $\chi > 0$, early-time uptake is greater, without forcing equilibrium to be reached unreasonably early. Adding a fitted χ to a model always resulted in a lower fitting error sum of squares, and generally decreased the bulk sand prediction error as well (Table 2). *Ball and Roberts*' [1991b] analysis of individual size classes allowed some fraction of the solute (up to 31%) to sorb instantaneously, in less than 0.01 day. This effectively added an additional fitting parameter to each size class, and increased early K_d^{app}/K_d^{ult} values, but provided no mechanism. As an alternative explanation, using fitted values of χ from our $7\mathcal{D}7\chi$ model, we see that for each size class, the fraction of total accessible volume that is within 1.5 μm of the particle's exterior is essentially ($r^2 = 0.97$) the same percent instantaneous sorption found by *Ball and Roberts* [1991b]. The point is not the specific distance we used, but rather that the value of the "instantaneous fraction" may be a consequence of that fraction of the total uptake capacity being within some distance or diffusion time from the exterior.

[46] The model improvement due to including connectivity nicely illustrates the persistent deviation between desorption measurements and theory discussed in section 1, although for sorption rather than desorption. Because the experiment involves sorption rather than desorption, chemical arguments regarding changes in the strength of the sorption are less convincing; pore connectivity issues provide a simple and coherent explanation.

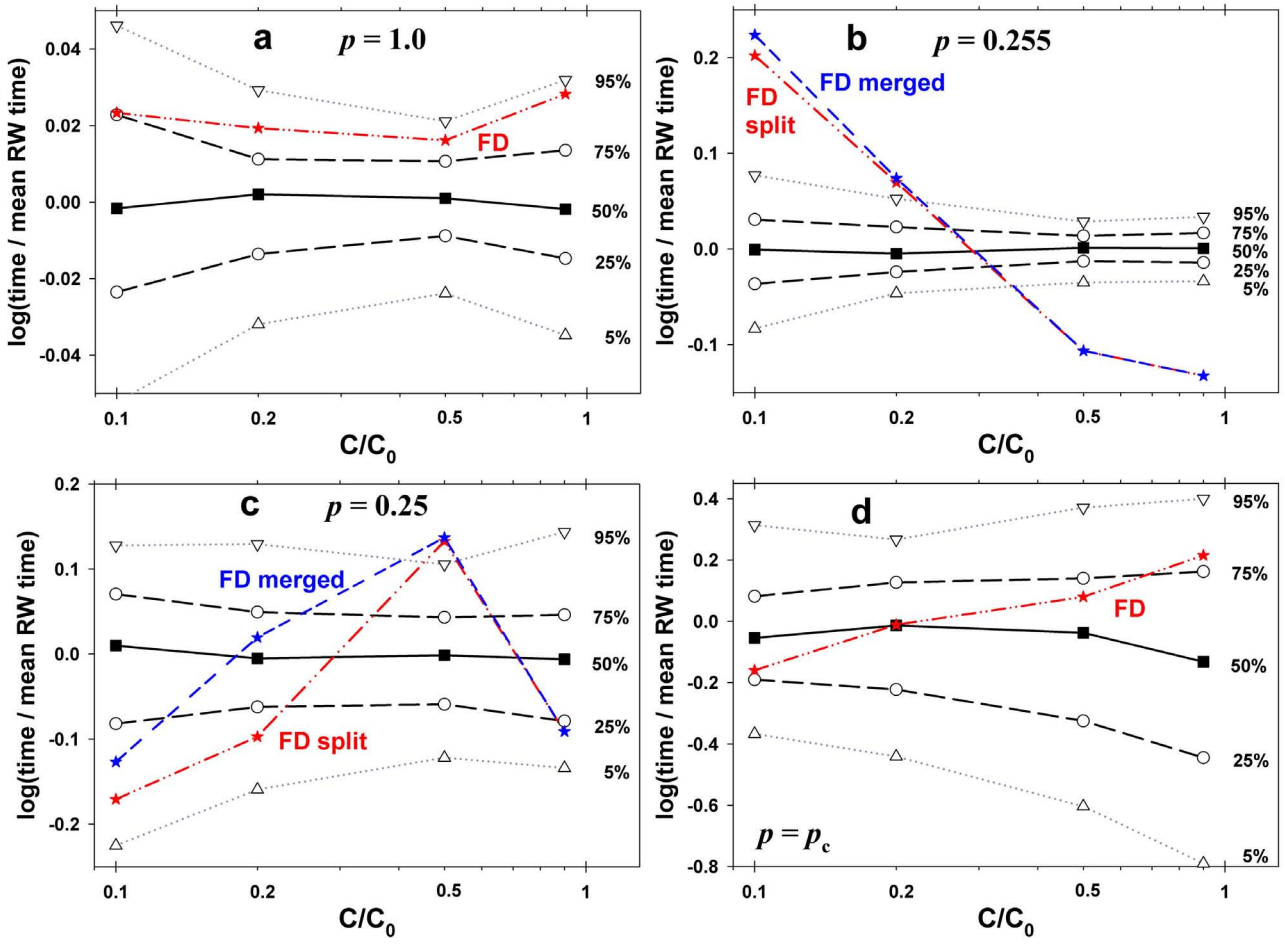

Figure 4. Finite difference (FD) flip times (times at which, during net in-diffusion, C/C_0 first reaches 10, 20, 50, and 90%) in comparison with selected percentiles of the distribution of flip times from the RW model. Connection probabilities are $p =$ (a) 1.0, (b) 0.255, (c) 0.25, and (d) p_c.

5. Discussion

[47] We now address more directly the issue raised by modifying equation (7) to account for finite-size effects. Clearly some modification was needed, because we cannot have $\mathcal{D}_{pm} = 0$ at $p = p_c$ in finite-size media. *Ewing et al.* [2010] observed (their Figure 10) that spheres having different radii behaved similarly over a range of connectivity values if $\chi < R$, but differences emerged when $\chi > R$. Comparing the mean flip times given by the RW model to those predicted by the FD model (Figure 8), we find that

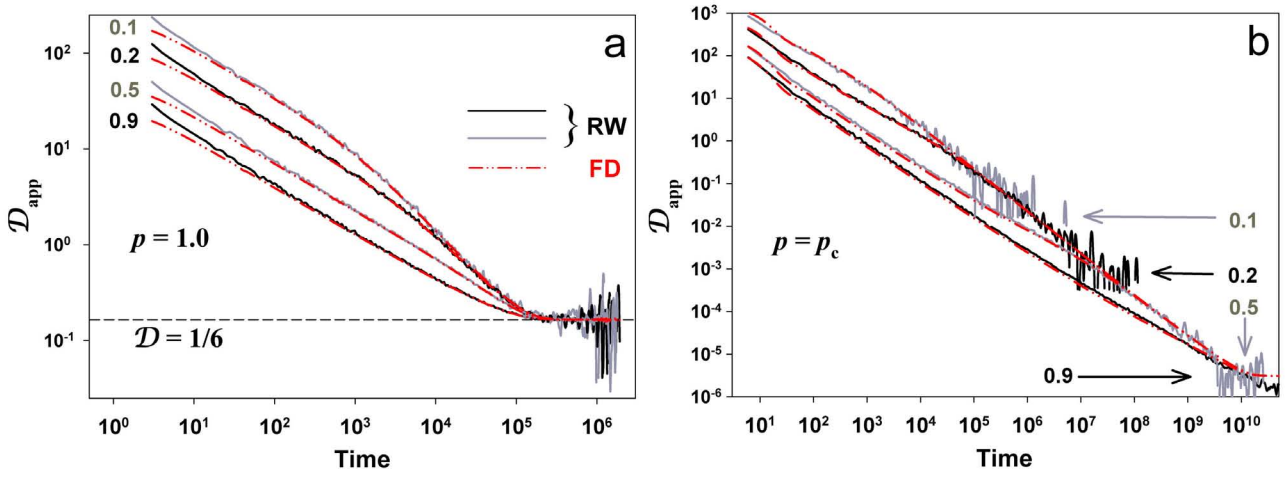

Figure 5. Apparent diffusion coefficient $\mathcal{D}_{app}$ as a function of time since the flip point, from RW simulations and the merged FD model, for (a) $p = 1.0$, and (b) $p = p_c$.

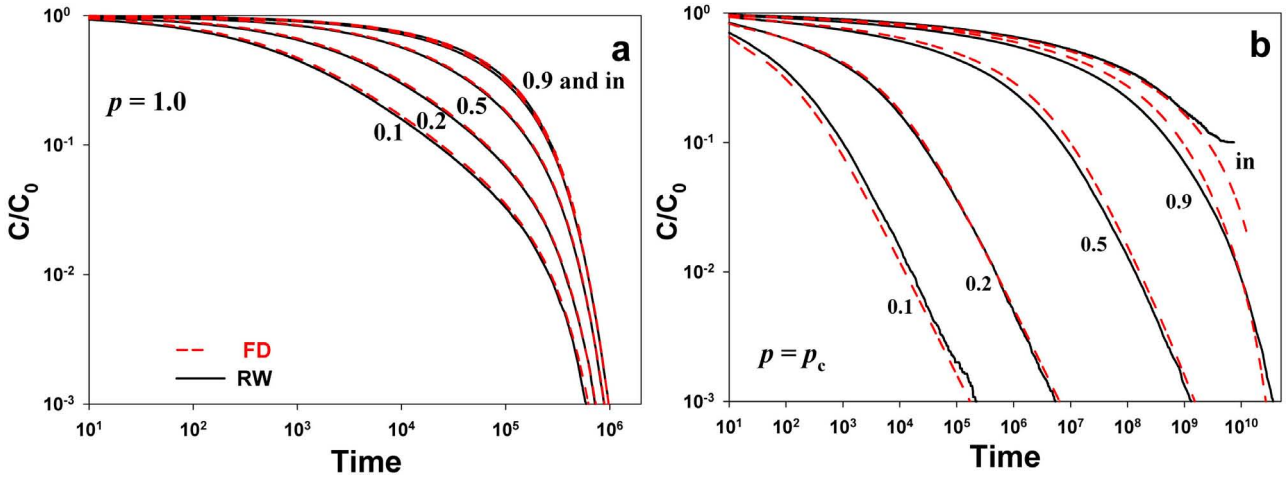

Figure 6. Comparison of RW and FD diffusion curves, all normalized to start at a mean internal concentration of 1.0. The in-diffusion curve, reversed as shown here, represents the case of starting at equilibrium. Spheres have $R = 500$ and $p =$ (a) 1.0, and (b) p_c.

the closest match, across all values of R, p, and C/C_0 compared, is always at $\chi = R$. Notice further that equation (8) describes the diffusion coefficient of the infinite cluster at distances $l > \chi$; at this distance there is no contribution from the finite clusters. But where $\chi > R$, such as for a finite sphere at p_c, the relevant length scale must be the system size R rather than the correlation length. This essentially forces all clusters to be finite, which requires modifying the percolation scaling; we conclude therefore that our modification (equation (8)) is reasonable and justified.

[48] It is instructive to compare the progress of diffusion in the two separate porosities (Figure 9). This figure uses the same properties used for Figure 1: $R = 500$ and $\chi = 250$. The finite clusters contribute about 2/3 of the total accessible pore volume, but C/C_0 of the whole sphere closely tracks C/C_0 in the finite clusters. The concentration in the infinite cluster lags far behind during net in-diffusion, indicating a lower diffusion coefficient—in fact, the apparent diffusion coefficient (via equation (16)) for the finite clusters is 3.5 to 80 times greater than that for the infinite cluster. But at any intragranular distance l, we expect the diffusion coefficient to be the same for the infinite cluster as it is for the finite clusters. What causes the slower response is a combination of two geometrical factors: first, the finite cluster pores are closer to the edge. For example, in the $R = 500$ sphere analyzed in Figure 1, 50% of the finite cluster accessible pore volume is within $l = 25$ of the edge, while getting to 50% of the infinite cluster accessible pore volume requires going into the sphere a distance $l = 147$. And second, most of the accessible pores at the edge belong to finite clusters, while the infinite cluster faces a bottleneck at that location. The excellent performance of the merged model suggests that this bottleneck effect, while an appealing argument, does not actually reflect what is happening in the sphere itself. A likely explanation is that those parts of the infinite cluster that are converted to finite clusters by the presence of the edge are dangling ends rather than the backbone itself.

[49] We now examine the common formalism for the diffusion coefficient, equation (1), in percolation terms for

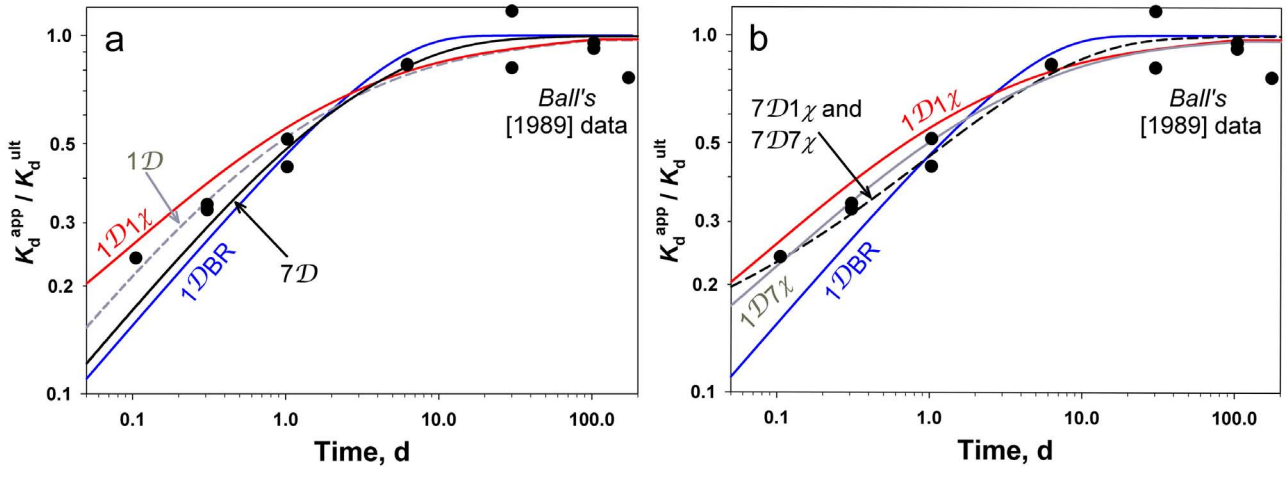

Figure 7. PCE uptake data from *Ball* [1989], and sorption modeled by (a) the $\chi = 0$ models and $1\mathcal{D}1\chi$, and (b) the $\chi > 0$ models and $1\mathcal{D}$BR. See Table 2 for model definitions and abbreviations.

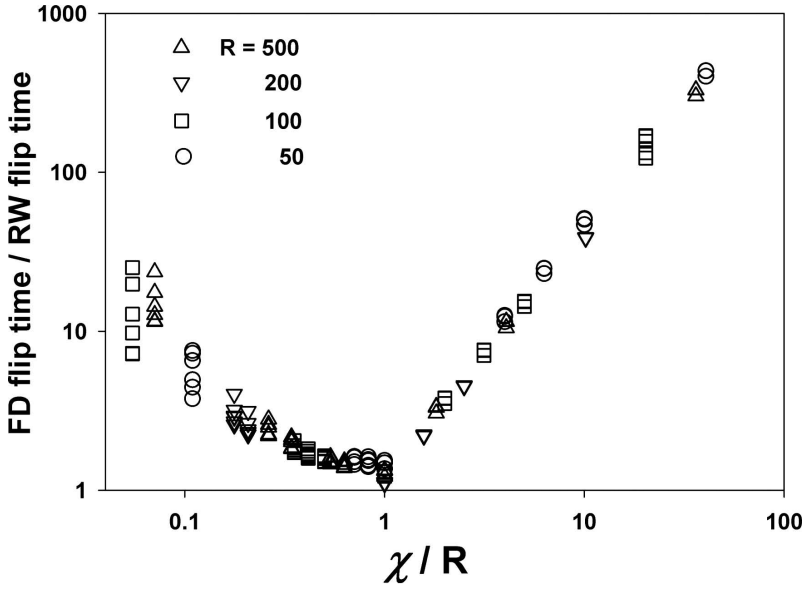

Figure 8. Ratio of FD flip time to RW median flip time, as a function of the ratio of the correlation length χ to the sphere radius R. Correlation lengths were altered by changing p^* (equation (8)). The best match of FD flip time to RW flip time was always obtained at $\chi = R$.

distances $l > \chi$. At these distances, the accessible porosity ϕ_a is entirely due to the infinite cluster, so it is given by $(p - p_c)^\beta$. Meanwhile, the tortuosity τ scales as the correlation length χ raised to the power $D_{min} - 1$ [*Ewing et al.*, 2010]. Incorporating these relationships into an expression for $\mathcal{D}_{pm}$ gives

$$\mathcal{D}_{pm}(p) \sim \frac{\phi_a}{\tau^2} \sim \frac{(p - p_c)^\beta}{\left([(p - p_c)^{-\nu}]^{D_{min}-1}\right)^2} = (p - p_c)^{\beta + 2\nu(D_{min}-1)}. \quad (17)$$

The resulting exponent has a value of approximately 1.008 in 3-D. That value is only about 3/4 of the value $\psi \equiv 2\nu - \beta \approx 1.35$ which gives the consistently strong match with the RW results seen in Figures 3–6. If we had not squared the tortuosity term, the exponent would be only about 0.71, barely half the correct value. This analysis emphasizes the importance of using equations with the correct exponents: an incorrect equation may perform adequately within a limited range, but its deviation from the correct response may become extreme as some limit (such as the percolation threshold) is unwittingly approached. Nonetheless, equation

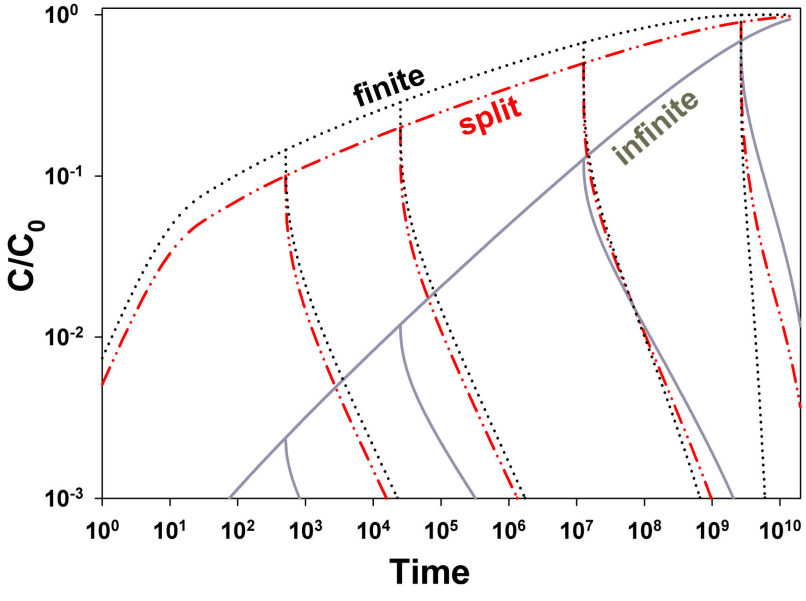

Figure 9. Internal concentration C/C_0 as a function of time for $R = 500$ and $\chi = 250$, shown separately for the finite clusters, the infinite cluster, and the sphere as a whole. The merged model (not shown) is essentially identical to the split model.

(1) still provides a fine intuitive explanation of why we expect $\mathcal{D}_{pm}$ to decrease with distance l into the rock.

[50] The concepts and methods developed here explain some heretofore puzzling aspects of diffusive mass transfer. Because this mass transfer can be a significant contributor to dispersion [*Haggerty and Gorelick*, 1995; *Gouze et al.*, 2008], non-Fickian behavior can significantly alter the long-term dispersion. We have shown that low intragranular pore connectivity is a plausible basis for non-Fickian mass transfer; this physical basis will improve understanding and aid development of new measurement and modeling methods. The concepts and methods presented here can be used directly as shown in analyzing the Borden sand data, used in a larger-scale simulation with individual spheres [e.g., *Tartakovsky et al.*, 2007], or applied to generate a memory function to inform mobile-immobile (MIM) or CTRW models [*Dentz and Berkowitz*, 2003; *Gouze et al.*, 2008]. While we have exclusively dealt with spherical geometry, the percolation relationships could also be used, e.g., to describe changes in a rock's accessible porosity and diffusion coefficient with distance from a fracture. The values of $p - p_c$ cannot be directly measured in a real rock, but its emergent macroscopic parameter χ is measureable. Several approaches to quantifying χ in natural rock have been pursued in our ongoing research.

6. Conclusions

[51] We develop a percolation-based FD model, test it against a rigorous set of RW simulations, and examine its use with real data. We conclude that:

[52] 1. The percolation relationships describing accessible porosity and diffusion coefficient (equation (2), and equation (9) or (11)) are fairly simple, and easily incorporated into an existing FD model.

[53] 2. Split and merged FD models give almost identical results. Parsimony therefore recommends the simpler merged model, although there may be cases where distinguishing between the infinite and finite components is useful.

[54] 3. The FD model produces results that compare well with the RW results, with a single fitting parameter and comparing over many orders of magnitude.

[55] 4. The FD model with two fitting parameters (χ and $\mathcal{D}_0$) performed well in modeling a physical system. Incorporating percolation effects into the FD model improved model predictions of PCE sorption into the Borden sand.

[56] 5. Comparison with the conventional formalism (equation (1)) shows why a percolation-based model is superior near p_c.

[57] 6. The exponent ψ for diffusion scaling with proximity to the percolation threshold is $2\nu-\beta$ ($\approx$1.35 in 3-D).

[58] 7. Low intragranular pore connectivity, if initiated at different degrees of diffusive nonequilibrium, can cause desorption to appear as if the solute has undergone slow sorption. That is, a solute's slow approach to intragranular equilibrium can present as progressively stronger sorption of the solute to the solid, even in the absence of any sorption process.

Notation

a prefactor for calculating χ, L.
b prefactor for calculating ϕ_a.
C solute concentration, M L^{-3}.
$\mathcal{D}$ diffusion coefficient, L^2 T^{-1}.
D_{min} percolation exponent.
FD finite difference (model).
K_d sorption coefficient, L^3 M^{-1}.
l distance from exterior of sphere, L.
PCE perchloroethene (tetrachloroethene).
p connection probability.
p_c critical connection probability.
p^* modified connection probability.
P fraction of sites belonging to the infinite cluster.
R sphere radius, L.
r distance from sphere center, L.
RW random walk (model).
S/L solid to liquid ratio for batch reactor, M L^{-3}.

Greek

α ratio of the volume of bulk solution in the batch reactor reservoir to the accessible intragranular volume, adjusted for sorption.
β percolation exponent.
Δ finite difference in value.
χ crossover length, L.
ϕ porosity.
λ chemical distance between two points, L.
τ tortuosity.
μ percolation exponent.
ν percolation exponent.
ϑ percolation exponent.
ψ percolation exponent.

Subscripts and Superscripts

a accessible from outside the particle.
app apparent and/or instantaneous; via macroscopic measurement.
aq aqueous.
c critical.
e at equilibrium.
f on the finite cluster(s).
i on the infinite cluster.
j index for radial position.
k known value.
p plateau, for distances $l > \chi$.
pm porous medium.
t index for time.
ult ultimate (at equilibrium).
0 initial or reference value.

[59] **Acknowledgments.** This research was partially supported by the Subsurface Biogeochemistry Research (SBR) Program, Office of Biological and Environmental Research (BER), U.S. Department of Energy (DOE), projects ER65073 and ER65074. A portion of the research was performed using EMSL, a national scientific user facility sponsored by DOE-BER and located at Pacific Northwest National Laboratory (PNNL). PNNL is operated for DOE by Battelle under contract DE-AC06-76RLO 1830. The authors thank Bill Ball for his many insightful comments.

References

Ball, W. P. (1989), Equilibrium sorption and diffusion rate studies with halogenated organic chemicals and sandy aquifer material, Ph.D. dissertation, Stanford Univ., Stanford, Calif.

Ball, W. P., and P. V. Roberts (1991a), Long-term sorption of halogenated organic chemicals by aquifer material, 1, Equilibrium, *Environ. Sci. Technol.*, *25*, 1223–1237.

Ball, W. P., and P. V. Roberts (1991b), Long-term sorption of halogenated organic chemicals by aquifer material, 2, Intraparticle diffusion, *Environ. Sci. Technol.*, *25*, 1237–1249.

Başağaoğlu, H., T. R. Ginn, and B. J. McCoy (2004), Radial pore diffusion with nonuniform intraparticle porosities, *J. Environ. Eng.*, *130*, 1170–1179.

Berkowitz, B., and I. Balberg (1993), Percolation theory and its application to groundwater hydrology, *Water Resour. Res.*, *29*, 775–794.

Brusseau, M. L., Q. Hu, and R. Srivastava (1997), Using flow interruption to identify factors causing nonideal contaminant transport, *J. Contam. Hydrol.*, *24*, 205–219.

Cornelissen, G., P. C. M. van Noort, and H. A. J. Govers (1997), Desorption kinetics of chlorobenzenes, polycyclic aromatic hydrocarbons, and polychlorinated biphenyls: Sediment extraction with Tenax® and effects of contact time and solute hydrophobicity, *Environ. Toxicol. Chem.*, *16*, 1351–1357, doi:10.1002/etc.5620160703.

Crank, J. (1975), *The Mathematics of Diffusion*, 2nd ed., Clarendon, Oxford, U.K.

Cunningham, J. A., and P. V. Roberts (1998), Use of temporal moments to investigate the effects of nonuniform grain-size distribution on the transport of sorbing solutes, *Water Resour. Res.*, *34*, 1415–1425.

Cunningham, J. A., C. J. Werth, M. Reinhard, and P. V. Roberts (1997), Effects of grain-scale mass transfer on the transport of volatile organics through sediments: 1. Model development, *Water Resour. Res.*, *33*, 2713–2726, doi:10.1029/97WR02425.

Dentz, M., and B. Berkowitz (2003), Transport behavior of a passive solute in continuous time random walks and multirate mass transfer, *Water Resour. Res.*, *39*(5), 1111, doi:10.1029/2001WR001163.

Epstein, N. (1989), On tortuosity and the tortuosity factor in flow and diffusion through porous media, *Chem. Eng. Sci.*, *44*, 779–781.

Ewing, R. P., and R. Horton (2002), Diffusion in sparsely connected pore spaces: Temporal and spatial scaling, *Water Resour. Res.*, *38*(12), 1285, doi:10.1029/2002WR001412.

Ewing, R. P., and A. G. Hunt (2006), Dependence of the electrical conductivity on saturation in real porous media, *Vadose Zone J.*, *5*, 731–741.

Ewing, R. P., Q. Hu, and C. Liu (2010), Scale-dependence of intragranular porosity, tortuosity, and diffusivity, *Water Resour. Res.*, *46*, W06513, doi:10.1029/2009WR008183.

Fleming, S. W., and R. Haggerty (2001), Modeling solute diffusion in the presence of pore-scale heterogeneity: Method development and an application to the Culebra dolomite member of the Rustler Formation, New Mexico, USA, *J. Contam. Hydrol.*, *48*, 253–276, doi:10.1016/S0169-7722(00)00182-0.

Gouze, P., Y. Melean, T. Le Borgne, M. Dentz, and J. Carrera (2008), Non-Fickian dispersion in porous media explained by heterogeneous microscale matrix diffusion, *Water Resour. Res.*, *44*, W11416, doi:10.1029/2007WR006690.

Haggerty, R., and S. M. Gorelick (1995), Multiple-rate mass transfer for modeling diffusion and surface reactions in media with pore-scale heterogeneity, *Water Resour. Res.*, *31*, 2383–2400.

Haggerty, R., and S. M. Gorelick (1998), Modeling mass transfer processes in soil columns with pore-scale heterogeneity, *Soil Sci. Soc. Am. J.*, *62*, 62–74.

Harmon, T. C., and P. V. Roberts (1994), Comparison of intraparticle sorption and desorption rates for a halogenated alkene in a sandy aquifer material, *Environ. Sci. Technol.*, *28*, 1650–1660, doi:10.1021/es00058a017.

Havlin, S., and D. Ben-Avraham (2002), Diffusion in disordered media, *Adv. Phys.*, *51*, 187–292.

Huang, W., P. Peng, Z. Yu, and J. Fu (2003), Effects of organic matter heterogeneity on sorption and desorption of organic contaminants by soils and sediments, *Appl. Geochem.*, *18*, 955–972.

Hunt, A. G. (2004), Percolative transport and fractal porous media, *Chaos Solitons Fractals*, *19*, 309–325.

Hunt, A. G., and R. P. Ewing (2009), *Percolation Theory for Flow in Porous Media, Lect. Not. Phys.*, 2nd ed., pp. 771, Springer, Berlin.

Hurvich, C. M., and C. L. Tsai (1995), Model selection for extended quasi-likelihood models in small samples, *Biometrics*, *51*, 1077–1084.

Liedl, R., and T. Ptak (2003), Modelling of diffusion-limited retardation of contaminants in hydraulically and lithologically nonuniform media, *J. Contam. Hydrol.*, *66*, 239–259, doi:10.1016/S0169-7722(03)00028-7.

Liu, C., J. M. Zachara, N. Qafoku, and Z. Wang (2008), Scale-dependent desorption of uranium from contaminated subsurface sediments, *Water Resour. Res.*, *44*, W08413, doi:10.1029/2007WR006478.

McGinley, P. M., L. E. Katz, and W. J. Weber, Jr. (1996), Competitive sorption and displacement of hydrophobic organic contaminants in saturated subsurface soil systems, *Water Resour. Res.*, *32*, 3571–3577.

Neretnieks, I. (1980), Diffusion in the rock matrix: An important factor in radionuclide retardation?, *J. Geophys. Res.*, *85*, 4379–4397.

Pedit, J. A., and C. T. Miller (1994), Heterogeneous sorption processes in subsurface systems: 1. Model formulations and applications, *Environ. Sci. Technol.*, *28*, 2094–2104, doi:10.1021/es00061a018.

Pignatello, J. J., and B. Xing (1996), Mechanisms of slow sorption of organic chemicals to natural particles, *Environ. Sci. Technol.*, *30*, 1–11, doi:10.1021/es940683g.

Press, W. H., S. A. Teukolsky, W. T. Vettering, and B. P. Flannery (1992), *Numerical Recipes in FORTRAN: The Art of Scientific Computing*, 2nd ed., Cambridge Univ. Press, Cambridge, U.K.

Ran, Y., W. Huang, P. C. S. Rao, D. Liu, G. Sheng, and J. Fu (2002), The role of condensed organic matter in the nonlinear sorption of hydrophobic organic contaminants by a peat and sediments, *J. Environ. Qual.*, *31*, 1953–1962.

Reichenberg, F., and P. Mayer (2006), Two complementary sides of bioavailability: Accessibility and chemical activity of organic contaminants in sediments and soils, *Environ. Toxicol. Chem.*, *25*, 1239–1245.

Sahimi, M. (1994), *Applications of Percolation Theory*, Taylor and Francis, London.

Stauffer, D., and A. Aharony (1994), *Introduction to Percolation Theory*, 2nd ed., Taylor and Francis, London.

Steinberg, S. M., J. J. Pignatello, and B. L. Sawhney (1987), Persistence of 1,2-Dibromomethane in soils: Entrapment in intraparticle micropores, *Environ. Sci. Technol.*, *21*, 1201–1208.

Tartakovsky, A. M., P. Meakin, T. D. Scheibe, and B. D. Wood (2007), A smoothed particle hydrodynamics model for reactive transport and mineral precipitation in porous and fractured porous media, *Water Resour. Res.*, *43*, W05437, doi:10.1029/2005WR004770.

Ten Hulscher, T. E. M., B. A. Vrind, H. van den Heuvel, P. C. M. van Noort, and H. A. J. Govers (2005), Influence of long contact times on sediment sorption kinetics of spiked chlorinated compounds, *Environ. Toxicol. Chem.*, *24*, 2154–2159, doi:10.1897/04-260R.1.

Warren, N., I. J. Allan, J. E. Carter, W. A. House, and A. Parker (2003), Pesticides and other micro-organic contaminants in freshwater sedimentary environments—A review, *Appl. Geochem.*, *18*, 159–194.

Werth, C. J. and K. M. Hansen (2002), Modeling the effects of concentration history on the slow desorption of trichloroethene from a soil at 100% relative humidity, *J. Contam. Hydrol.*, *54*, 307–327, doi:10.1016/S0169-7722(01)00183-8.

Werth, C. J., and M. Reinhard (1997), Effects of temperature on tricholorethylene desorption from silica gel and natural sediments. 2. Kinetics, *Environ. Sci. Technol.*, *31*, 697–703.

Zachara, J., C. Brown, J. Christensen, J. A. Davis, E. Dresel, C. Liu, S. Kelly, J. McKinley, J. Serne, and W. Um (2007), A site-wide perspective on uranium geochemistry at the Hanford Site, *Rep. PNNL-17031*, 224 pp., Pacific Northwest Natl. Lab., Richland, Wash.

R. P. Ewing, Department of Agronomy, Iowa State University, Ames, IA 50011, USA. (ewing@iastate.edu)

Q. Hu, Department of Earth and Environmental Sciences, University of Texas at Arlington, 500 Yates St., MS 19049, Arlington, TX 76019, USA. (maxhu@uta.edu)

C. Liu, Chemical and Materials Science Division, Fundamental and Computational Science Directorate, Pacific Northwest National Laboratory, PO Box 999, MSIN K8-96, Richland, WA 99352, USA. (chongxuan.liu@pnnl.gov)